Second International Conference on CFD in the Minerals and Process Industries
CSIRO, Melbourne, Australia
6-8 December 1999

THREE-DIMENSIONAL MODELLING OF INDUSTRIAL GRANULAR FLOWS

Paul W. CLEARY and Mark L. SAWLEY

CSIRO Mathematical and Information Sciences, Clayton, Victoria 3169, AUSTRALIA

ABSTRACT

The Discrete Element Method (DEM) is attracting increasing interest for the simulation of industrial granular flows. While the majority of previous DEM modelling has considered two-dimensional flows, we present here a series of three-dimensional simulations for a number of important industrial applications. The charge motion in a 5m diameter ball mill and in a Hicom nutating mill, discharge from single- and four-port cylindrical hoppers, and particle size separation by a vibrating screen are considered. For each case, realistic particle size distributions have been used. The results obtained indicate that DEM modelling is now sufficiently advanced that it can make useful contributions to process optimisation and equipment design.

INTRODUCTION

The flow of particulate materials is a critical part of many industrial and mining processes. These range from crushing and grinding, blasting, separation (as in mineral liberation) and mixing (such as in glass making), to rotary moulding of plastics, commodity sampling (frequently from conveyor belts at discharge or interchange points), stockpile construction and discharge, open cut mining, excavation (including dragline operation) to generic particle flows in and from hoppers, silos, bins and conveyor belts. Small reductions in energy consumption or increases in output represent significant financial benefits for plant owners.

In the simulation of granular flows using the Discrete Element Method (DEM) the trajectories, spins and orientations of all the particles are modelled, as are their interactions with other particles and with their environment. This method has been well established for simple flows for many years (Campbell, 1990; Barker, 1994; Walton, 1994). Many industrial applications have been successfully modelled in two dimensions, such as dragline excavators (Cleary, 1998a), ball mills (Mishra and Rajamani, 1992, 1994; Cleary, 1998b), silo filling (Holst et. al., 1997) and a wide selection of industrial applications in Cleary (1998c).

Three-dimensional DEM modelling of industrial applications has received little attention in the literature, because of the scale of the problems combined with complexity of the industrial geometries. Typical minimum problem sizes range from 20,000 to 100,000 particles with larger problems having millions of particles and the largest substantially more. Rapidly increasing computer speed and the advent of production parallel DEM codes allow these problems to be explored.

In this paper we describe simulations of several large-scale, geometrically-complex industrial applications. Issues of importance for large-scale three-dimensional DEM simulations, including generating initial conditions, code parallelisation, and visualisation, are discussed.

THE DISCRETE ELEMENT METHOD

DEM simulation involves following the motion of every particle in the flow and modelling each collision between particles and between particles and the environment. Equations of motion are also solved for the boundary objects with which the particles interact in order to treat moving boundaries. Industrial applications place heavy demands on the geometrical capabilities of DEM codes; this is particularly true for three-dimensional geometries.

Boundary objects are constructed by either extruding two-dimensional cross sections made from arbitrary line segments, circular segments or discs or from three-dimensional, triangular finite-element surface meshes. These meshes can be provided by any reasonable mesh generator using geometries imported from a CAD package. This provides enormous flexibility in specifying the environment with which the particles interact. As is the case for two-dimensional modelling, rigid body and surface motions can be specified for the three-dimensional simulations. External forces, such as cables for supporting the dragline buckets, can be attached to the objects.

The particles are currently modelled as spheres and can be either added during the simulation as a stream of particles or can be built into stationary groups of particles by extruding packed two-dimensional microstructures into three-dimensional arrays. Each such group can be composed of any number of subgroups whose range of diameters, densities and material properties can be independently specified according to selected probability distributions.

The particles are allowed to overlap and the amount of overlap Δx and normal v_n and tangential v_t relative velocities determine the collisional forces. There are a number of possible contact force models available that approximate the collision dynamics to various extents.

The same linear spring-dashpot model as used in previous two-dimensional modelling is employed for the three-dimensional simulations reported in this paper. The normal force

$$F_n = -k_n \Delta x + C_n v_n \ ,$$

consists of a linear spring to provide the repulsive force and a dashpot to dissipate a proportion of the relative kinetic energy. The maximum overlap between particles is determined by the stiffness k_n of the spring in the normal direction. Typically, average overlaps of 0.1-1.0% are desirable, requiring spring constants of the order of 10^6-10^7 N/m. Note that the spring constants required to achieve these target overlaps are lower than in two dimensions, since the force exerted on particles is proportional to their masses, and the mass of a spherical particle is much smaller than that of a cylinder of unit length. The normal damping coefficient C_n is chosen to give the required coefficient of restitution ε (defined as the ratio of the post-collisional to pre-collisional normal component of the relative velocity), and is given in Cleary (1998c).

The tangential force is given by

$$F_t = \min\left\{\mu F_n, k_t \int v_t dt + C_t v_t\right\},$$

where the vector force F_t and velocity v_t are defined in the plane tangent to the surface at the contact point. The integral term represents an incremental spring that stores energy from the relative tangential motion and models the elastic tangential deformation of the contacting surfaces, while the dashpot dissipates energy from the tangential motion and models the tangential plastic deformation of the contact. Depending on the history of the contact, it is possible for the spring to be loading in one direction and simultaneously unloading in the orthogonal direction. The total tangential force F_t is limited by the Coulomb frictional limit $\mu F_{n,}$, at which point the surface contact shears and the particles begin to slide over each other.

The discrete element algorithm has three main stages:

- A search grid is used to build periodically a particle near-neighbour interaction list. Using only particle pairs in the near neighbour list reduces the force calculation to an *O(N)* operation, where N is the total number of particles. Industrial simulations with 100,000 particle are thus possible in reasonable times on current workstations. The search needs to be more sophisticated for three-dimensional simulations than in two dimensions in order to avoid the search procedure becoming the dominant cost of the algorithm. In particular, finding neighbours efficiently when there is a large range of particle sizes is critical.
- The collisional forces on each of the particles and boundary objects are evaluated efficiently using the near-neighbour list and the spring-dashpot interaction model, and then transformed into the simulation frame of reference.
- All the forces and torques on the objects and particles are summed and the resulting equations of motion are integrated. Time integration is performed using a second-order predictor-corrector scheme and typically uses between 10 and 50 time steps to integrate accurately each collision. This leads to very small time steps (typically 10^{-3} to 10^{-6} s depending on the controlling length and time scales of each application).

BALL MILL

Ball mills are large rotating drums (up to around 5 m in diameter) used for grinding rock in the mineral processing and quarrying industries. The rock generally comes from a crusher or perhaps a semi-autogenous (SAG) mill (depending on the design of the milling circuit) and is fed into one end of mill. Grinding media consisting of steel balls with sizes in the range 5 to 20 cm are present in the mill along with rock that is still too large to exit through the extraction grate at the opposite end. Particles migrate slowly along the length of the mill, while circulating rapidly with the mill shell in the plane orthogonal to the mill axis. The radial and azimuthal particle motion is assisted by lifter bars attached to the mill shell. Replaceable liner plates are bolted to the shell between the lifters to reduce wear in this hostile environment.

A typical 5 m diameter ball mill consumes around 3 to 4 MW of power and has an energy efficiency of around only 1 to 5%. Significant economic and environmental benefits can be obtained by improving this efficiency even slightly. There are also significant costs involved in replacing the liners (commonly made from expensive, wear-resistant, cast molybdenum stainless steel) arising both from the liner replacement cost and from lost production. Further significant benefits can be obtained through higher downstream recovery if the exit particle size distributions can be made closer to the optimum for the subsequent flotation processes.

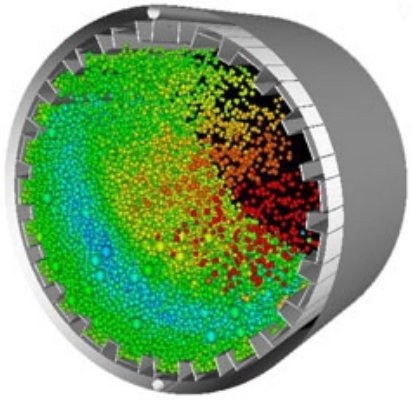

Figure 1: Instantaneous locations of the balls (coloured by velocity) in a ball mill.

Here we consider the motion of the steel balls in a 3 m axial section of the same 5 m ball mill that has been used in previous two-dimensional simulation (Cleary, 1998b). There are 23 lifter bars attached around the circumference of the mill and running the full length of the mill. The mill geometry is effectively two dimensional, but extruded along its axis of rotation. The mill rotates clockwise at some fraction *N* of the critical rotation rate of 19.5 rpm (based on the 4.8 m internal diameter of the liner), at which an average size ball begins to centrifuge. The charge of 30,000 particles is comprised of 5% (by number) of 200 mm, 47.5% of 100 mm and 47.5% of 75 mm diameter spherical balls, and corresponds to a solid loading of 50%. Periodic boundaries are assumed at the axial ends of the simulation domain, so that the model represents an infinitely long mill.

Figure 1 shows the positions of the balls (coloured by their velocity) in a mill rotating at N=80%. Qualitatively, the flow pattern is quite similar to that observed for the two-dimensional case (Cleary, 1998b). The toe is on the right and the charge shoulder is elevated on the left. Particles near the mill shell rotate almost rigidly with the mill rotation, until they reach the shoulder. The particles between the lifters are hurled into space and form a well-defined cataracting layer high in the mill. These particles impact heavily on the charge in the toe region and against the liner above. The bulk of the particles avalanche down the steeply inclined slope of the charge. Between the avalanching layer in the middle and the rigidly rotating layer on the outside is a stationary region. The very high shear produced between these layers leads to particle size reduction of rocks in the ball mill by abrasive rubbing, chipping off of sharp corners of the rocks, and by small particles being pinched between the balls.

HICOM NUTATING MILL

The grinding process in a Hicom 120 mill is achieved through a unique combination of the grinding chamber geometry and a high-speed nutating motion. Centrifugal accelerations of up to 50G and power densities up to 2500 kW/m^3 can be generated, resulting in very high particle breakage rates. Hicom mills can be used for a variety of comminution tasks (Hoyer and Boyes 1994; Hoyer and Morgan 1996), and are particularly well suited to energy-efficient, fine grinding down to 10 microns and below.

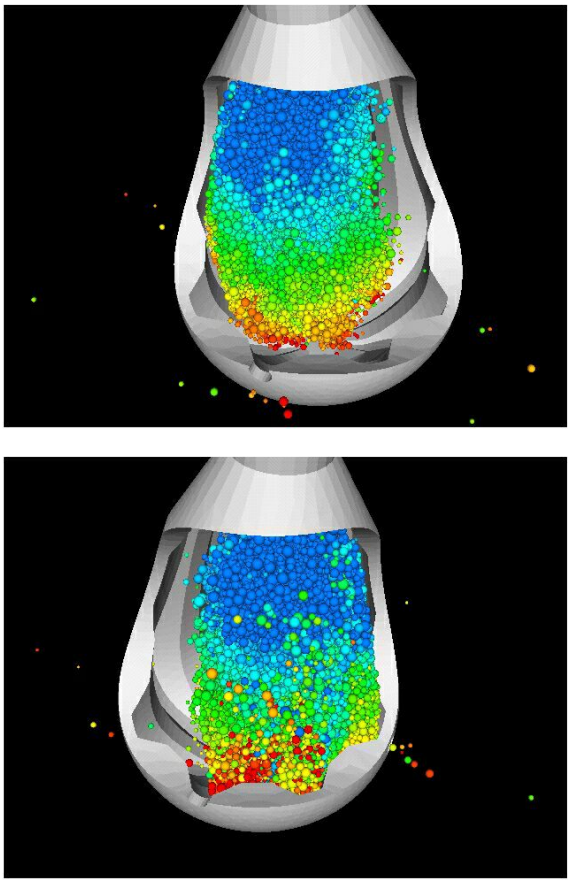

Figure 2: Side cutaway view, at two different times, of the particles (coloured by velocity) in the Hicom nutating mill.

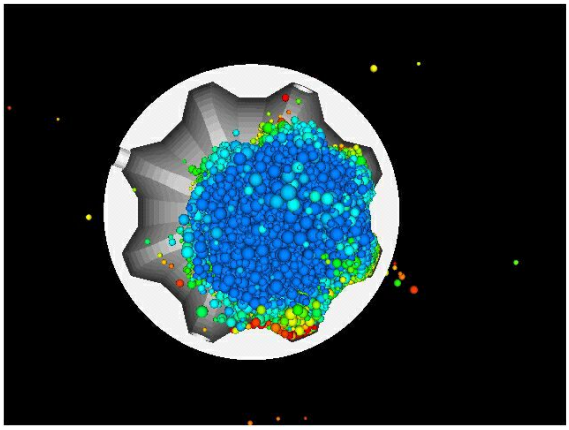

Figure 3: Top cutaway view of the particles (coloured by velocity) in the Hicom nutating mill.

Insights into the complex motion of the mill charge have been obtained through DEM simulations. In the present study, the grinding chamber is inclined at an angle of 4.75 degrees from vertical, and moves with a nutating motion at a frequency of 730 rpm. In performing this motion, the nutation point at the top of the chamber remains stationary, while points on the chamber below describe circles of diameter increasing with distance from the nutation point. The grinding chamber, which is roughly conical in shape with a hemispherical base, is filled at the top through a 120 mm diameter port. Ground material is discharged through four equally-spaced ports in the side of the chamber. For the present simulations, the 60-litre chamber was half-filled with 22,600 spherical particles of size uniformly distributed between 6 and 20 mm diameter.

Figure 2 shows two snapshots of the mill with a cutaway view from the side. The particles (coloured by velocity) are forced against the interior side wall of the mill by the centrifugal force and are somewhat slumped towards the bottom in response to the comparatively weak gravitational force. As the chamber rotates, the particle charge moves around the inside of the mill. This generates the high shear between particles that results in the grinding process. The motion of the particles is more gentle in the upper section of the mill, since the centrifugal force is comparatively low. In the lower section, the chamber is wider and its displacement from the vertical (caused by the inclination) is larger, leading to much higher particle accelerations and much higher speed impacts. The impact of the particles at the leading edge of the charge with the raised internal ribs is particularly strong. As the charge mass moves over a section of chamber wall containing a discharge port, a pulse of particles is emitted.

Figure 3 shows the cutaway view from the top of the mill chamber. The rib pattern of the mill liner is clearly observed, as is the shape of the charge. This shape remains relatively invariant, merely rotating with the mill rotation. At the specific time chosen for this figure, a group of particles can be seen just outside the mill having just exited from the lower right discharge port.

SIZE SEPARATION BY A VIBRATING SCREEN

Vibrating screens are commonly used to separate particles according to their size. Separation is a critical step in most mineral processing operations and the efficiency of this separation has direct implications for both mineral recovery levels and costs.

Particle segregation by one level of a screen is presented here. We consider a 800 mm square screen, 10 mm thick, containing a 12x12 array of 40 mm square holes. The screen is covered by a mixture of 8,000 spherical particles, with sizes uniformly distributed between 10 and 60 mm, to a depth of 400 mm. Periodic boundaries have been applied at each of the sides of the screen to simulate a screen having a much larger area. The screen is oscillated upwards and to one side with a frequency of 3 Hz, a vertical amplitude of 50 mm, and a sideways amplitude of 20 mm. The oscillations in the two directions are in phase so that the screen moves sinusoidally in a straight line inclined at 22 degrees to the vertical.

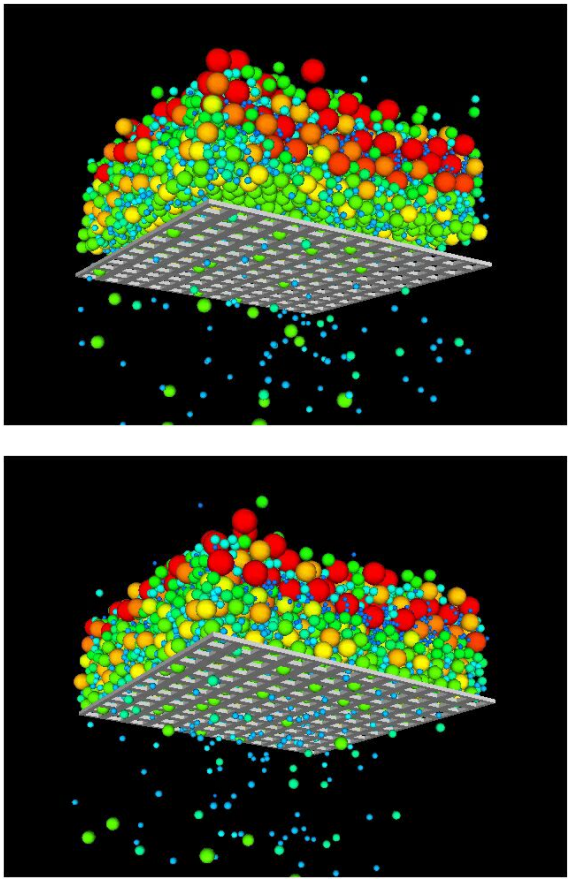

Figure 4: Particle locations (coloured by size) at two different times during the vibration cycle of the screen.

Figure 4 shows the screen at two times during the vibration cycle. As it moves upwards, smaller particles (shaded blue through to green) move freely through the holes in the screen. The flow of small particles continues throughout the screen's upward movement, although the rate declines slightly. As the screen moves down, the particles lag behind and loose contact with the screen. The flow of small particles through the screen abates until the screen reaches its lowest point and the particles crash back into the screen producing a surge of smaller particles through the screen. This behaviour leads to a regular pulsing flow of fines from the screen. Also observed in Figure 4 is the well-defined size segregation of the material on top of the screen, with the larger (red) particles being dominant near the upper surface. The progressive percolation of small particles from the upper regions to the region adjacent to the screen ensures a continual supply of fines to flow through the screen. The ability of DEM to simulate this type of flow demonstrates the method's potential for use as a design tool for such industrial particle handling equipment.

DISCHARGE FROM A CYLINDRICAL HOPPER

Hoppers are often used for particle storage in the mineral processing and manufacturing industries. They consist of large storage areas with some type of discharge region below. A particularly common type is a cylindrical hopper with a single central discharge port.

DEM simulations have been undertaken for a cylindrical hopper, 3 m high and 1.5 m in diameter, having a discharge port of 400 mm diameter. The hopper chute angle of the conical section is 45 degrees. The particles are uniformly distributed in size between 40 and 80 mm diameter, with 25,000 required to fill the hopper.

Figure 5 shows the location of the particles (coloured by initial vertical position) at one time during the discharge. In this view the particles and the hopper have been cut away to show details of the particle distribution within the centre of the hopper. Even at this early time during the discharge, the preferential flow down the centre of the hopper is clearly discernible.

Many materials will not flow in hoppers with such shallow hopper chute angles. In order to avoid excessively tall structures, it is quite common to have multiple discharge ports from multiple conical sections with a much steeper chute angle. Multiple discharge ports can also be used if large ranges of flow rates are required or if the material needs to flow to different destinations.

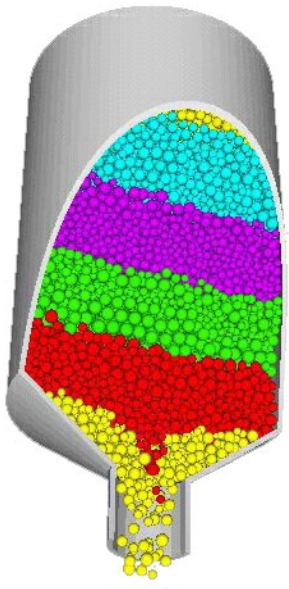

Figure 5: Cutaway view of the discharging of particles (coloured in layers) from a cylindrical single-port hopper.

DEM simulations have been performed for a cylindrical four-port hopper, 4 m high and 1.5 m in diameter. The four discharge ports each have a diameter of 250 mm and a conical chute angle of 60 degrees. The particles are uniformly distributed in size between 25 and 60 mm. For this case, 70,000 particles are required to fill the hopper, and particles discharge through all four ports.

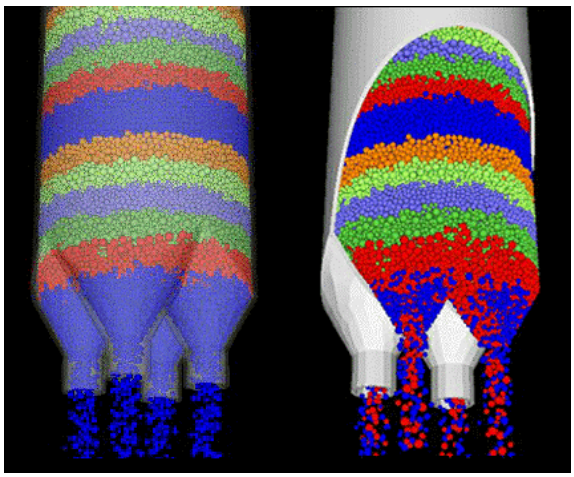

Figure 6: Two views, at different times, of discharging of particles (coloured in layers) from a cylindrical four-port hopper.

Figure 6 shows two representative views at different times during the simulation. Again, the particles are coloured by their initial vertical position. The view on the left of Figure 6 shows the hopper as translucent to enable the behaviour of the particles adjacent to the hopper shell to be studied. On the right of Figure 6 is shown a cutaway view that allows the behaviour of the closest particles to be more easily identified.

DEM modelling can be used to assess the effect of using only some of the discharge ports and to assess the impact of various combinations of these on the forces applied by the flowing granular material to the hopper structure. The existence of stagnant regions can also be identified along with other impediments to flow, which are much more common in multiple discharge hoppers.

PARALLELISATION

Since the above DEM simulations involve a relatively modest number of spherical particles (<100,000), the computations were able to be performed in a reasonable time on a single-processor workstation. As the geometric and physical complexity of the modelling increases, so does the computational resources required. The simulation of, for example, one million non-spherical particles in a complex 3D geometry, including the effects of breakage and/or cohesion, is thus not reasonably performed by a single processor. However, the required level of computational power can, in principle, be obtained through the application of parallel computing to the DEM simulations.

As a preliminary study of the development of a parallel DEM code, the parallelisation of two-dimensional simulations has been investigated. The underlying parallel algorithm is based on domain decomposition. The simulation domain is divided into subdomains by a simple slicing parallel to either the x or y axis. Choosing the number of subdomains equal to the number of processors available, data associated with particles in the same subdomain are stored in the same processor's memory. The computational effort depends on the number of collisions between particles, which is closely related to the number of particles. Assuming processors of equal performance, to achieve load balance (in order to minimise synchronisation delays), the subdomains are chosen to contain the same number of particles.

Of the different parallel programming models available, message passing (using either the MPI or PVM library) has been chosen for the present implementation. This model provides both low communication overhead (leading to higher parallel performance) and a high level of code portability (since message passing is available on essentially all parallel computer systems). Communication between processors associated with interactions of particles across the subdomain boundaries is optimised by copying a layer of "ghost" particles from the neighbouring subdomains, as shown in Figure 7.

Using the above-described parallel algorithm, after the input data is read and distributed to the appropriate processor memory, each processor performs essentially the same grid search and collision calculation as for the sequential algorithm. Periodic communication between processors is necessary to update the ghost cell information. It is important to note that the subdomain boundaries are not fixed in physical space, but are automatically moved to satisfy the load balancing requirements. Such dynamic load balancing is essential for an efficient parallel DEM implementation.

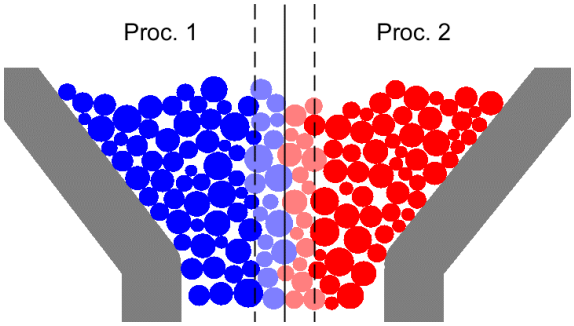

Figure 7: Particles coloured according to storage location in memory for a two-processor decomposition. Light colours denote ghost particles.

The performance of this parallel implementation has been assessed on the Swiss-T0 machine, consisting of a cluster of 8 Digital Alpha 21164 processors (Gruber, 1998); the Fast Ethernet interconnect was used for the present study. Figure 8 shows, on a log-log plot, the measured wall-clock time required to simulate 1 s (about 5500 time steps) of the flow of 10,000 particles in a 2D hopper. It can be observed that the time required to build the near-neighbour search list and to calculate the collisional forces decreases linearly with the number of processors employed. The construction of the search grid, which involves inter-processor communication, requires a time roughly independent of the number of processors. However, since the grid construction is not excessively

time-consuming (for up to the 8 processors used), the total simulation time is seen to decrease essentially linearly with the number of processors.

While only a maximum of 8 processors have been used for this performance study, it should be noted that large 3D flow simulations will involve significantly more particles than has been considered here. Since the ratio of communication to computation time decreases with particle numbers, it is anticipated that such large 3D simulations will yield close to linear scaling for substantially greater numbers of processors interconnected via a suitable low-latency network.

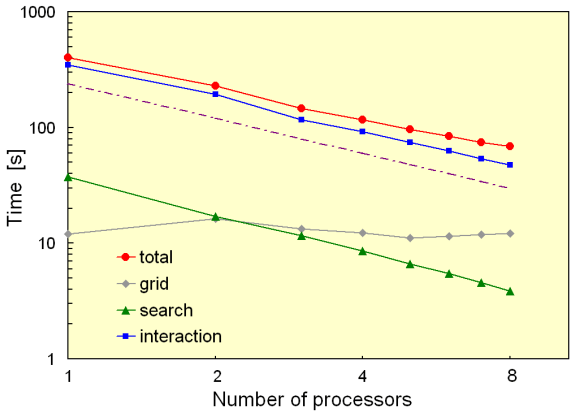

Figure 8: Computational time required for the individual tasks of a 2D DEM simulation. The dashed line represents linear scaling.

PRE-PROCESSING AND VISUALISATION

The examples presented above illustrate the type of geometric complexity that is required to be modelled in industrial applications. We have chosen to implement in our simulation procedure a strategy utilising as much commercial pre-processing software as possible. The geometry is initially constructed using a CAD package (e.g. AutoCAD). This geometry is then imported into a commercial mesh generator (e.g. FEMAP) to construct a standard triangular finite-element surface mesh that then describes the object for the DEM code. (A tetrahedral mesh describing the geometry volume may also be required for visualisation purposes.) Particle-object contact detection then reduces to efficient particle triangular primitive contact detection.

Visualisation of such particulate flows is extremely difficult because of the requirement to render the surfaces of all the particles. Even relatively simple cases, such as the ball mill with 30,000 particles, require around 3 million polygons to be computed for each time frame. Of these polygons, very few are seen since all but the front particles are obscured. Most commercial CFD visualisation software is unable to distinguish between the particles needed to be drawn and those which are not. Such 3D simulations can take almost as long to visualise as they do to compute. Thus, while parallel DEM simulations involving around a million particles are computationally feasible, they still provide an immense challenge for visualisation.

CONCLUSION

The 3D modelling capabilities of our DEM code have been described along with the difficulties that arise from generating the geometries and visualising the resulting particulate systems. The methodology used to parallelise the DEM code has also been discussed.

The examples that have been presented indicate that DEM modelling is now sufficiently advanced that it can make useful contributions to process optimisation and equipment design. Simulations of the charge flow in a 5 m ball mill and a nutating mill demonstrate that complicated geometries executing complex motion can be modelled easily. Simulations of flow through a vibrating screen and discharge from single- and four-port cylindrical hoppers illustrate the potential of DEM to handle diverse aspects of particle handling equipment.

ACKNOWLEDGEMENTS

The study of the Hicom nutating mill were performed under contract with CH Warman Techlink. Access to the Swiss-T0 computer system at the Ecole Polytechnique Fédérale de Lausanne is gratefully acknowledged.

REFERENCES

BARKER, G.C., 1994, "Computer simulations of granular materials", in *Granular Matter: An Inter-disciplinary Approach*, A. Mehta (ed.), Springer-Verlag.

CAMPBELL, C.S., 1990, "Rapid granular flows", *Ann. Rev. Fluid Mech.*, **22**, 57-92.

CLEARY, P.W., 1998a, "The filling of dragline buckets", *Math. Eng. in Indust.*, **7**, 1-24.

CLEARY, P.W., 1998b, "Predicting charge motion, power draw, segregation, wear and particle breakage in ball mills using discrete element methods", *Minerals Eng.*, **11**, 1061-1080.

CLEARY, P.W., 1998c, "Discrete element modelling of industrial granular flow applications", *TASK. Quarterly - Scientific Bulletin*, **2**, 385-416.

GRUBER, R. and DUBOIS PÈLERIN, 1998, "Swiss-Tx: First experiences on the T0 system", *EPFL Supercomputing Review*, **10**, 19-23.

HOYER, D.I. and BOYES, J.M., 1994, "High-intensity fine and ultrafine grinding in the Hicom mill", *Proc. XV CMMI Congress* (Johannesburg), *SAIMM*, **2**, 435-441.

HOYER, D.I. and MORGAN, R.E., 1996, "High-intensity size reduction in the Hicom mill", *Proc. Chemeca 96* (Sydney).

HOLST, J.M., ROTTE, J.M., OOI, J.Y. and RONG, G.H., 1997, "Discrete particle and continuum modelling of particulate solids in silos: SILO FILLING", *Research report R97-007, Dept. of Civil and Environmental Engineering, University of Edinburgh, Edinburgh, UK*

MISHRA, B.K. and RAJAMANI, R.K., 1992, "The discrete element method for the simulation of ball mills", *App. Math. Model.*, **16**, 598-604.

MISHRA, B.K. and RAJAMANI, R.K., 1994, "Simulation of charge motion in ball mills. Part 1: experimental verifications", *Int. J. Mineral Process.*, **40**, 171-186.

WALTON, O.R., 1994, "Numerical simulation of inelastic frictional particle-particle interaction", in *Particulate Two-Phase Flow*, M.C. Roco (ed.), Butterworth-Heineman, Chpt. 25, 884-911.